

## Atomic force microscopy of living and fixed *Xenopus laevis* embryos

Yu.M. Efremov<sup>a</sup>, E.A. Pukhlyakova<sup>b,\*</sup>, D.V. Bagrov<sup>a</sup>, K.V. Shaitan<sup>a</sup>

<sup>a</sup> M.V. Lomonosov Moscow State University, Faculty of Biology, Department of Bioengineering, 111991, Leninskie Gory, 1/73, Moscow, Russia

<sup>b</sup> M.V. Lomonosov Moscow State University, Faculty of Biology, Department of Embryology, 111992, Leninskie Gory, 1/12, Moscow, Russia

### ARTICLE INFO

#### Article history:

Received 14 December 2010

Received in revised form 27 May 2011

Accepted 31 May 2011

#### Keywords:

Atomic force microscopy (AFM)

Scanning electron microscopy (SEM)

*Xenopus laevis* embryo

### ABSTRACT

*Xenopus laevis* embryos are a rather simple and at the same time a very interesting animal model, which is widely used for research in developmental biology. Intensive coordinated cell movements take place during the multi-cellular organism development. Little is known of the cellular, molecular and biomechanical mechanisms of these movements. The conceptual framework for analysis of cell interactions within integrated populations is poorly developed. We have used atomic force microscopy (AFM) to observe the surface of fixed *X. laevis* embryos at different stages of their development. We have developed a new sample preparation protocol for these observations. The obtained images were compared with scanning electron microscopy (SEM) data. Cell rearrangement during morphogenesis *in vivo* was also visualized by AFM. In the current paper we discuss facilities and challenges of using this technique for further embryo researching.

© 2011 Elsevier Ltd. All rights reserved.

### 1. Introduction

The embryos of *Xenopus laevis*, a South African clawed toad, are widely used in biological research (Gurdon and Hopwood, 2000). They are a convenient model for the study of developmental mechanisms and protein functions because of the large embryo size and simplicity of manipulation.

Traditionally, the surface morphology of *X. laevis* embryos has been studied by scanning electron microscopy (SEM) (Tarin, 1971). Although electron microscopy techniques such as SEM and transmission electron microscopy reach nanometer and subnanometer resolution, they need complex and invasive sample treatments that may significantly modify the native structure.

AFM has become a powerful tool for many biological studies, including the imaging of biological macromolecules (Engel and Muller, 2000; Graham et al., 2010), cells (Cai et al., 2009; Rotsch and Radmacher, 2000) and force measurements (Butt et al., 2005; Kuznetsova et al., 2007; Vinckier and Semenza, 1998). The AFM provides three-dimensional images of the surface topography of the studied specimens at nanometer resolution and can image samples both in air and in liquid. The latter provides an opportunity to study biological objects (e.g. cells, tissues, biomacromolecules, etc.) in physiological environment. Moreover, dynamic processes can be studied with AFM (Engel and Muller, 2000). Increasing the image

acquisition speed allows one to capture molecular dynamic processes with AFM (Ando et al., 2003; Suzuki et al., 2011). However there are only few AFM investigations of fresh tissue explants (for example, Jurvelin et al., 1996; Kreplak et al., 2007; Miyazaki and Hayashi, 1999; Reichlin et al., 2005; Tsilimbaris et al., 2000) and virtually no such research on a whole living organism, since most researchers work with cell cultures (Braet and Wisse, 2004; Rotsch et al., 1999; Rotsch and Radmacher, 2000). In our work living *X. laevis* embryos at gastrula stage have been visualized by AFM. We have shown that AFM allows cell movement visualization on the embryo surface *in vivo*.

Research of *X. laevis* embryos by AFM has been described, but not enough. According to the published data, only the oocyte stage was analyzed. So far AFM imaging of nuclear envelope (Oberleithner et al., 2000; Shahin et al., 2005), plasma membrane (Lal and Yu, 1993; Lau et al., 2002; Orsini et al., 2006, 2009, 2010; Santacrose et al., 2008; Schillers et al., 2000), vitelline envelope (Solletti et al., 1994) and cortical cytoskeleton (Santacrose et al., 2006) of *X. laevis* oocytes has been reported in the literature. In this work for the first time AFM has been used to visualize the surface of fixed *X. laevis* embryos at different stages of their development.

Cell rearrangement is a fundamental mechanism of multi-cellular organism development. The structure, fates, and morphogenetic movements of the prospective tissues through gastrulation and neurulation are geometrically complex, however the understanding of these events is fundamental to the understanding of nearly all aspects of early development (Kay, 1991). They represent a category of morphogenetic processes, the so-called “mass movements”, and present a major challenge and an opportunity to understand cell functions in the morphogenesis of the integrated

\* Corresponding author. Tel./fax: +7 495 9395738.

E-mail addresses: [yu.efremov@gmail.com](mailto:yu.efremov@gmail.com) (Yu.M. Efremov), [ekaterinapoooh@gmail.com](mailto:ekaterinapoooh@gmail.com) (E.A. Pukhlyakova), [dbagrov@gmail.com](mailto:dbagrov@gmail.com) (D.V. Bagrov), [shaitan@moldyn.org](mailto:shaitan@moldyn.org) (K.V. Shaitan).

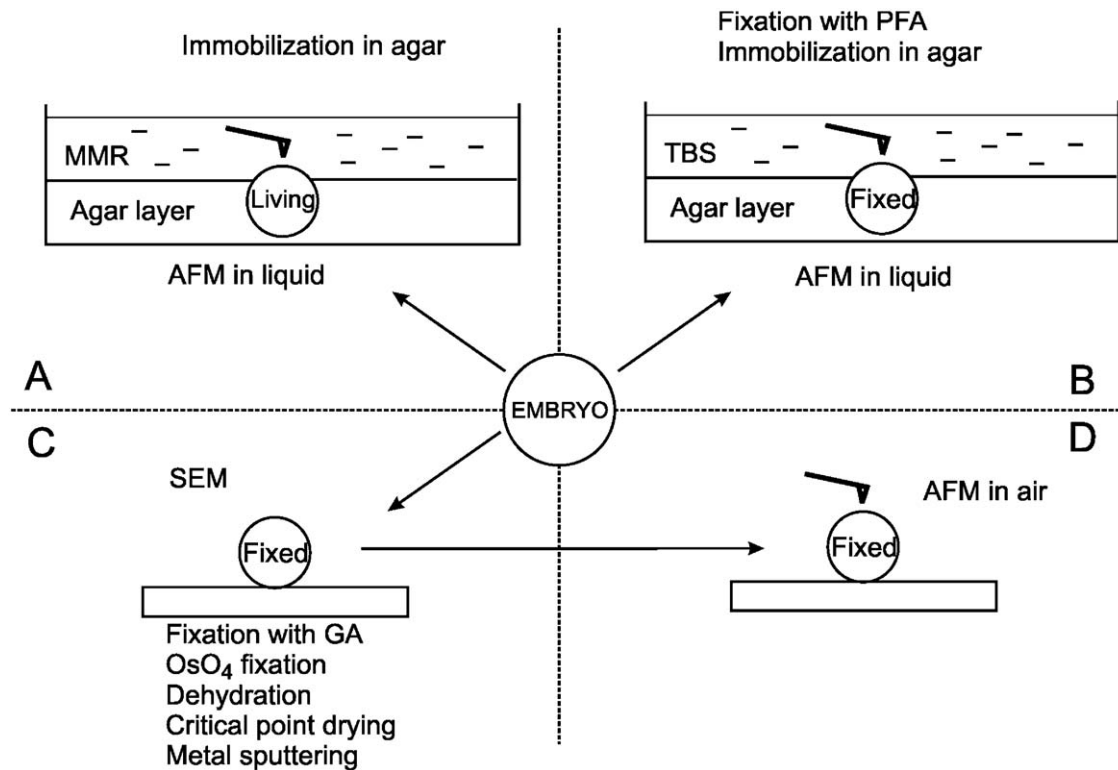


**Fig. 1.** Scheme of the experiment. (A) Living and (B) PFA fixed embryos at different stages were placed in the holes in the agar layer and visualized with AFM in liquid. Samples fixed with GA and OsO<sub>4</sub>, dehydrated, critical point dried and metal sputtered were studied with (C) SEM and (D) AFM in air.

populations. The common paradigm for the morphogenesis investigation is the study of individual cell motility in culture at low density. In contrast, most cell movements in embryos involve high densities of cells interacting with one another, or with the extracellular matrix between them (Keller et al., 2000). *X. laevis* embryo is a suitable model system to study cell rearrangement and movement during morphogenesis.

The current work consists of two parts. In the first part fixed *X. laevis* embryos at different stages of development were imaged by AFM, the results were compared with SEM data (both our own and taken from the literature). In the second part living *X. laevis* embryos were imaged and cell rearrangements were visualized.

## 2. Materials and methods

### 2.1. Preparation of embryos

Eggs were obtained from *X. laevis* females previously injected with human chorionic gonadotropin and fertilized with sperm from testis stored at 4 °C (Keller, 1975). Jelly coats were removed with a brief treatment in 2% cysteine hydrochloride solution (DiaM, Switzerland), pH 8 (Keller, 1981). Embryos were cultivated in a 10% MMR solution (0.1 M NaCl (Avogadro, Moscow, Russia), 2 mM KCl (Reachim, Russia), 2 mM CaCl<sub>2</sub> (Serva Feinbiochemica, Heidelberg), 1 mM MgSO<sub>4</sub> (Avogadro, Moscow, Russia), 5 mM HEPES (DiaM, Germany), pH 7.2) and staged according to (Nieuwkoop et al., 1967). Vitelline envelopes were stripped away with forceps immediately prior to visualization.

### 2.2. Sample preparation for AFM

Fixation of embryos was performed for 2 h with 4% paraformaldehyde (Pancreac, Barcelona, Spain) in TBS solu-

tion (50 mM Tris–HCl, pH 7.4 and 150 mM NaCl) with the following immobilization in agarose and AFM imaging. A small holes of approximately embryo sizes in diameter (~1 mm) and a half of embryo size in depth were made by the thin needle in the 2% agarose (Applichem, Darmstadt, Germany) layer prepared in Petri dishes. The rest of the dish volume was filled with either 10% MMR or TBS solution for visualization living (Fig. 1A) and fixed (Fig. 1B) embryos respectively. Embryos were placed and tightly held in the holes made in the agarose layer. The projecting part of the embryo had a hemispherical form, and lateral sides of this hemisphere had a big slope. The flattest place on the hemisphere, which was the most proper area for AFM analysis, was the top of the hemisphere. When the embryo was immobilized in agarose, it was turned to make the region of interest (e.g. animal or vegetal pole) to be looked up. Such immobilization method did not affect the living embryo, because they could develop normally after prolonged (5–6 h) experiment. So this technique may be recommended for the embryo research. A schematic image of the main embryo stages studied is shown on Fig. 2. A similar protocol has been described (Solletti et al., 1994). According to that protocol, conical hole in plexiglass with a film of silicon grease and pipette with gelatine were used for mounting oocytes, but these methods are more complicated and less reliable (oocytes came off the pipette easily during imaging, silicon grease is not good environment for living embryos).

### 2.3. Atomic force microscopy

Atomic force microscopy imaging was performed using a Solver BIO Olympus atomic force microscope (NT-MDT, Zelenograd, Russia) with a scanning field of 100 μm × 100 μm × 7 μm. Images of 256 × 256 or 512 × 512 pixels were obtained at scan rate 0.5–1.5 Hz. The scan size was chosen taking into account that the embryo has

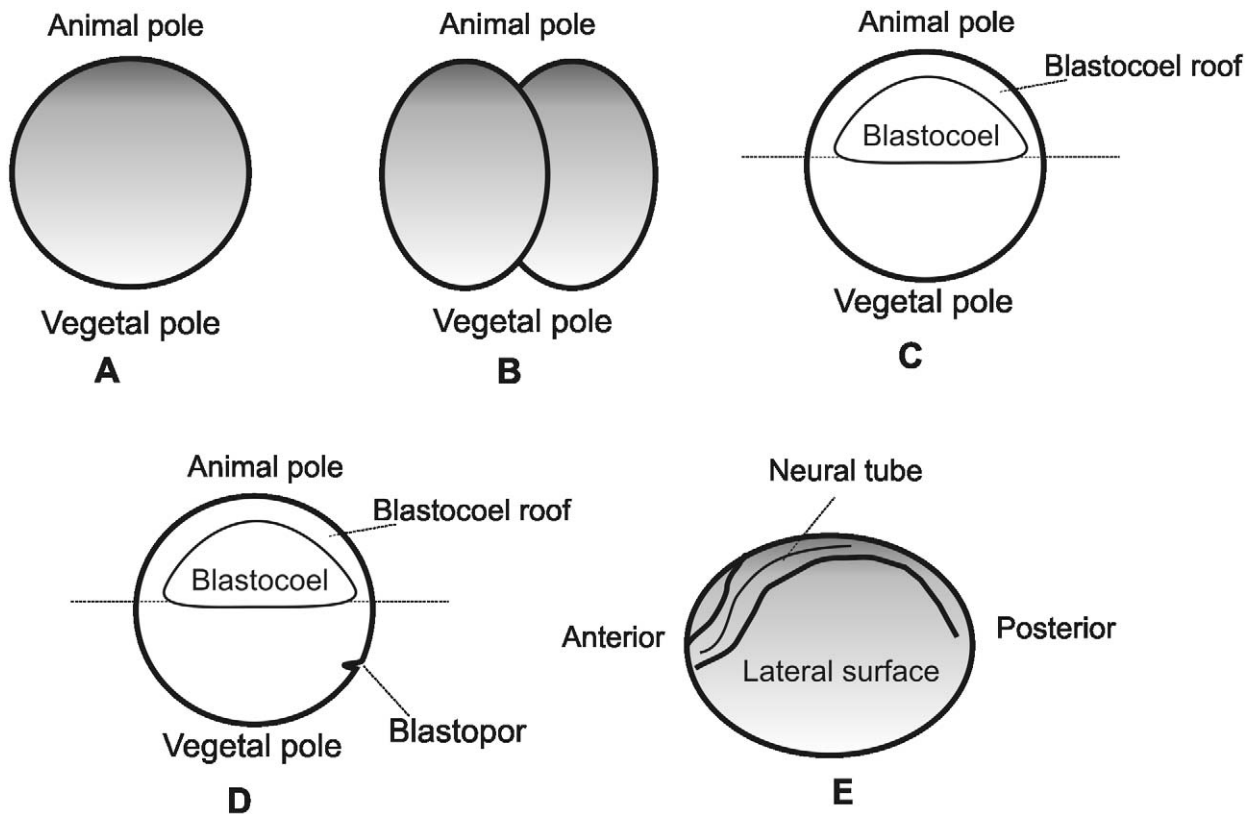


**Fig. 2.** Schematic image of the main embryo stages studied. (A) Zygote (st. 1). (B) Early cleavage (st. 2). (C) Sagittal section of blastula (st. 9). (D) Sagittal section of gastrula (st. 10). (E) Neurula (st. 14).

a spherical form, and its surface has large variations of height on lateral sides, so the AFM scanning range in the vertical direction is not always sufficient for the measurements. It was usually possible to obtain images about  $40\ \mu\text{m} \times 40\ \mu\text{m}$ , and up to  $80\ \mu\text{m} \times 80\ \mu\text{m}$  on the top of the hemisphere.

Images were obtained in contact mode in liquid with the use of rectangular and triangular silicon nitride cantilevers Veeco MSCT-AUHW (Veeco Instruments, Santa Barbara, California). For imaging living and fixed embryos cantilevers with force constant  $0.01\text{--}0.02\ \text{N/m}$  and  $0.03\text{--}0.05\ \text{N/m}$  respectively were used. The use of the semicontact mode did not provide any additional information about the surface, neither has it increased the quality of the images, so only the contact mode was used (see [Supplementary data](#)). However, semicontact mode was used in air to study samples prepared for SEM (see below, [Fig. 1D](#)), cantilevers NSG01 (NT-MDT, Zelenograd, Russia) were used.

The procedure for atomic force microscope imaging in the contact mode in liquid for biological material has been described elsewhere ([Braet and Wisse, 2004](#)). The loading force applied on the sample during imaging was approximately  $1\text{--}4\ \text{nN}$  for living and up to  $8\ \text{nN}$  for fixed embryos as measured by the force/distance curves. In contact mode trace and retrace height images and error signal images (cantilever deflection) were registered simultaneously. The comparison of the trace and retrace sections served as a criterion of the consistency of the data and quality of the feedback operation. Scanning parameters (feedback gain, interaction force, scanning speed) were chosen to make the trace and retrace sections coincide with a minimal error. The error signal helped to reveal subtle heterogeneity of the surface ([Rotsch and Radmacher, 2000](#)).

The acquired images were processed (flattened by second order line-wise fit) using Image Analysis software (NT-MDT, Zelenograd, Russia) and FemtoScan Online (Advanced technologies centre,

Moscow, Russia). Measurements in horizontal and vertical plane were made using the section analysis tool.

The quantitative data are typically presented as mean  $\pm$  standard deviation. The values were measured on images of several embryos (at least three) with subsequent averaging over them. The number of analyzed structures was  $N \sim 50\text{--}80$  in each measurement.

#### 2.4. Scanning electron microscopy

Embryos were fixed in 2.5% glutaraldehyde (Merck, Germany) in TBS solution, pH 7.3 for 12 h,  $4^\circ\text{C}$ , and postfixed for 1 h, RT in 0.5%  $\text{OsO}_4$  in the same buffer solution. Samples were dehydrated using a graded series of the dehydration agent (ethanol followed by acetone). They were dried with a critical point apparatus (the transitional fluid was  $\text{CO}_2$ ) and sputtered with a  $\sim 20\ \text{nm}$  layer of Au/Pd compound for SEM imaging (SEI, Camscan-S2, Cambridge Instruments) ([Fig. 1C](#)).

### 3. Results and discussion

#### 3.1. Research of fixed *X. laevis* embryos at different stages of embryogenesis

##### 3.1.1. Zygote and early cleavage (stages 1–3)

AFM images of both animal and vegetal pole surfaces of the zygote, two- and four cell embryos were obtained. At these stages the embryo surface topography is defined mainly by microvilli ([Monroy and Baccetti, 1975](#)). On SEM images microvilli on the animal pole looked like round elongated protrusions ([Fig. 3D](#)), and on the vegetal pole they have ripple shape ([Fig. 4D](#)).

Similar structures were observed if samples were prepared for SEM and scanned by AFM in air in semi-contact mode ([Fig. 1D](#)). On

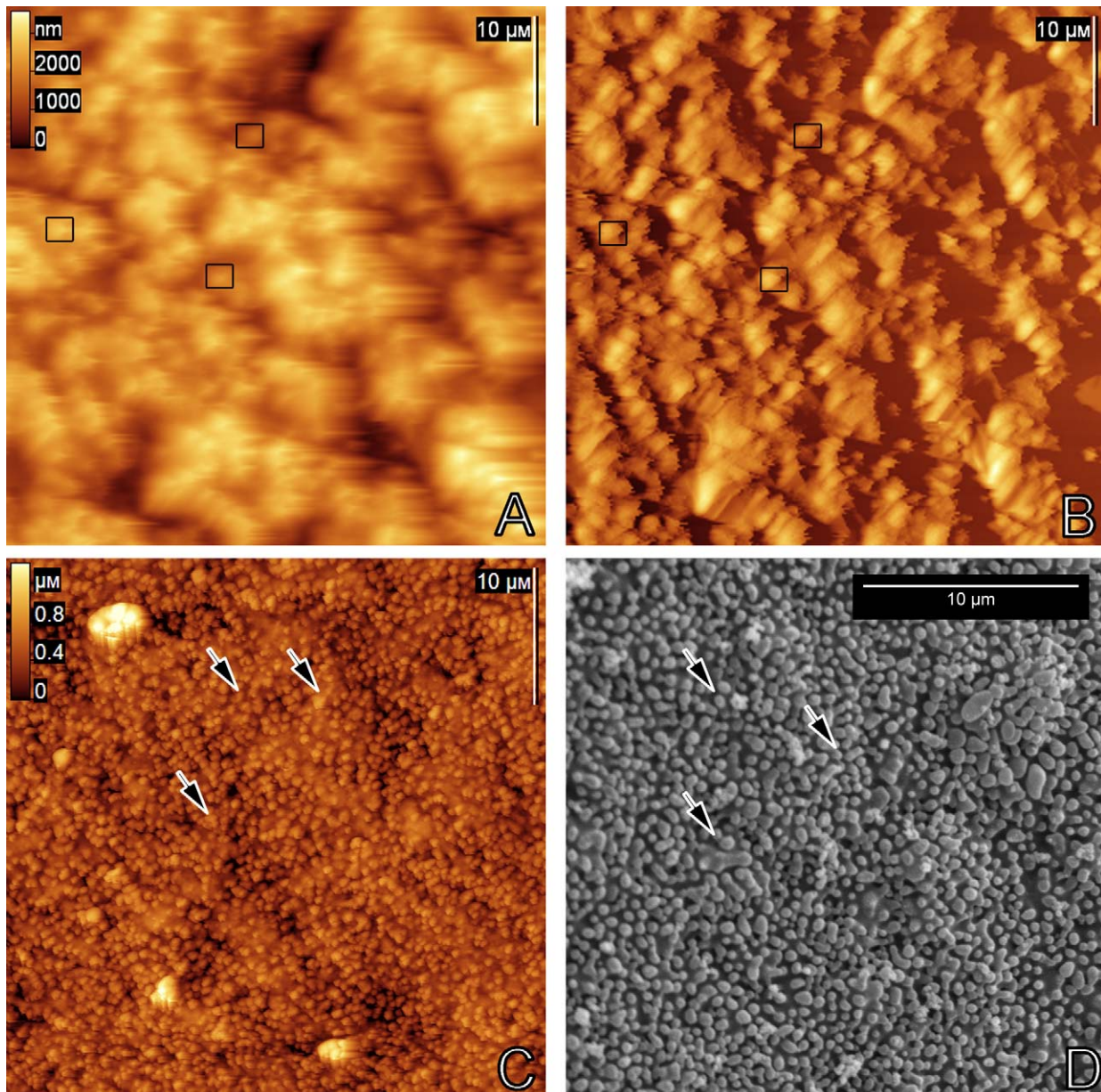


**Fig. 3.** Fixed zygote (st. 1), animal pole. Contact mode AFM in liquid: (A) topography and (B) error signal images. (C) AFM image (semicontact mode in air), received on the sample, prepared for SEM. (D) Scanning electron micrograph. Arrows on (C) and (D) show some of the protrusions on the surface, which are interpreted as microvilli. Boxes on (A) and (B) indicate some of the protruding areas, which are interpreted as yolk granules.

the animal pole microvilli have a  $380 \pm 100$  nm height,  $490 \pm 90$  nm width and typical density  $\sim 3 \mu\text{m}^{-2}$  (Fig. 3C). The rippled microvilli on the vegetal pole have a  $230 \pm 80$  nm height and  $390 \pm 70$  nm width (Fig. 4C). Widths were measured at half-height. It should be noticed, that here and later the real width is 50–70 nm smaller than the measured value owing to tip broadening (Ricci and Braga, 2004). In this case the broadening also caused by metal coating ( $\sim 20$  nm). Some protruding areas shown in Fig. 4C by black boxes may be interpreted as yolk granules. Still we cannot prove that suggestion because the borders of the granules are not clearly visible under densely packed microvilli.

However, when AFM images were obtained in liquid on fixed embryos, hemispherical bodies on the membrane surface but not the microvilli, were observed both on animal (Fig. 3A and B) and vegetal (Fig. 4A and B) poles. The hemispherical bodies are  $1.4 \pm 0.9 \mu\text{m}$  diameter,  $17 \pm 4$  per  $100 \mu\text{m}^2$  density on the animal pole and  $2.9 \pm 1.4 \mu\text{m}$  diameter and  $23 \pm 6$  per  $100 \mu\text{m}^2$  density

on the vegetal pole. These bodies were marked by black boxes (Figs. 3 and 4). The tip can sweep them along the scan direction, so their shape is distorted (Fig. 4A and B). The use of the semicontact mode did not increase the quality of the images (see Supplementary data). Similar structures were also observed on later stages (shown below). We interpreted them as yolk granules, which are 0.5–6  $\mu\text{m}$  size (Monroy et al., 1976). The microvilli were not observed with AFM at these developmental stages, probably because of their high density on the surface (Solletti et al., 1994). They are mobile and thus cause instabilities of the tip-sample interaction during the imaging process. It is shown below, that at the later stages the microvilli density decreases and they can be imaged by AFM without additional preparation.

From a two-cell stage the surface becomes smoother, the quantity of microvilli decreases. Some of them are believed to merge with the membrane (Denis-Donini et al., 1976), and the remained microvilli concentrate where the division furrow will appear. Pre-

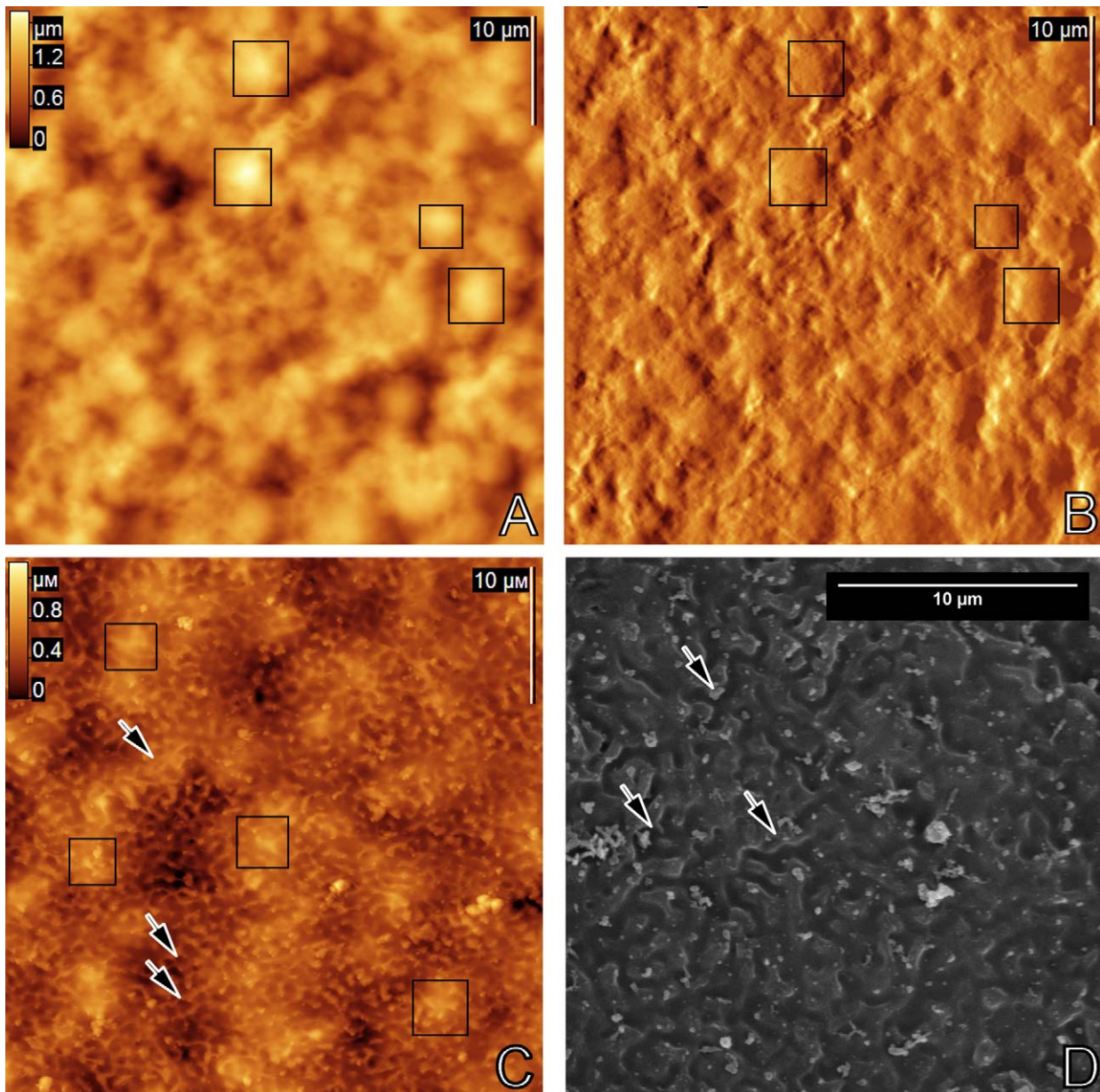


**Fig. 4.** Fixed zygote (st. 1), vegetal pole. Contact mode AFM in liquid: (A) topography and (B) error signal images. (C) AFM image (semicontact mode in air), received on the sample, prepared for SEM. (D) Scanning electron micrograph. Arrows on (C) and (D) show some of the ripples on the surface, which are interpreted as microvilli. Boxes on (A)–(C) indicate some of the protruding areas, which interpreted as yolk granules.

sumably, they are located where the new membrane material merges with the surface (during division the membrane area increases by 26–28%) (Denis-Donini et al., 1976).

The membrane ultrastructure of two-, four-cell embryos and zygote observed by AFM is similar at these stages (data not shown). This similarity was observed when imaging both in air and in liquid. Imaging of the later cleavage embryos (up to blastula stage) is complicated because of the deep cleavage furrows and because less area is available for scanning.

### 3.1.2. Blastula (stage 9)

Continued cleavage forms an embryo with numerous small cells in the animal region and a relatively small number of large, yolky cells in the vegetal region. A superficial cell layer on the animal pole forms the epithelium which seals off the inner cavity, called blastocoel, from the outside by tight intercellular junctions (Fig. 2C). The blastocoel increases its volume and the blastocoel roof expands uni-

formly in cell movement called epiboly. The diameter of the embryo increases during blastulation, largely because of the expansion of the blastocoel roof (Keller, 1980).

The surface looks rough because of yolk granules inside the cells on the AFM images (Fig. 5A and B). They are visualized as hemispherical bodies ( $1.0 \pm 0.4 \mu\text{m}$  width,  $350 \pm 180 \text{ nm}$  height,  $13 \pm 3$  per  $100 \mu\text{m}^2$  density on the animal pole, and  $2.5 \pm 1.7 \mu\text{m}$  width,  $340 \pm 130 \text{ nm}$  height,  $13 \pm 4$  per  $100 \mu\text{m}^2$  density on the vegetal pole (data not shown)). On the animal pole in the area of cell boundaries, which look like furrows, small poles about  $1 \mu\text{m}$  in diameter and  $0.5 \mu\text{m}$  in depth are visible. Similar holes on the SEM data (Fig. 5C) are interpreted as artifacts of fixation (Monroy et al., 1976), and they are not observed on the living embryos (see below). So, we suggest that holes, observed also on the later stages, are artifacts of fixation.

On SEM images, yolk granules are also observed on the surface ( $\sim 0.5 \mu\text{m}$  on the animal pole (Fig. 5C), and  $2.5\text{--}6 \mu\text{m}$  on the

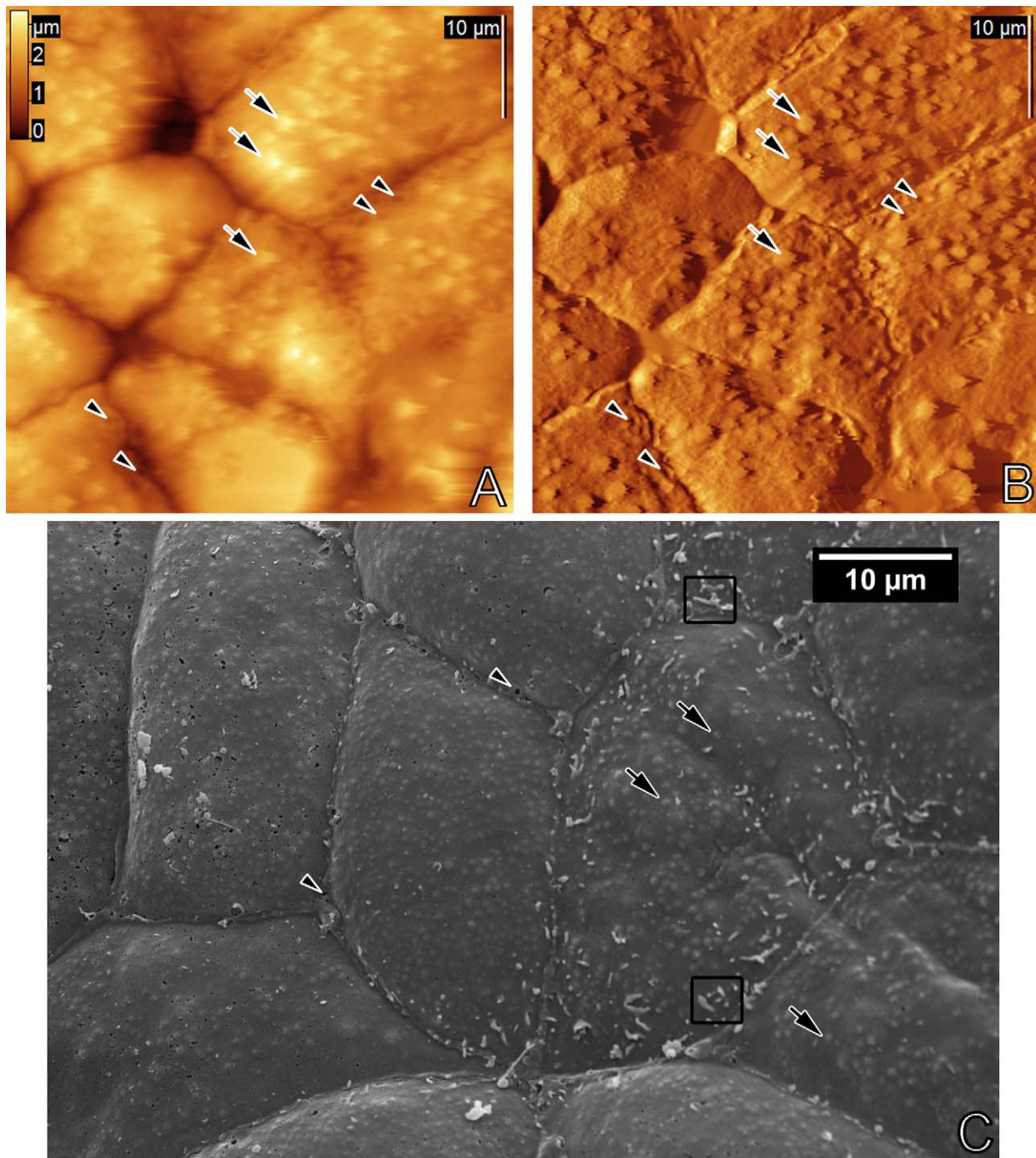


**Fig. 5.** Fixed blastula (st. 9), animal pole, contact mode AFM in liquid: (A) topography and (B) error signal images. (C) Scanning electron micrograph. Arrows indicate the yolk granules, triangular pointers show small poles in the area of the cell boundaries. Boxes on SEM image indicate some areas with microvilli.

vegetal pole (data not shown)). These data correspond with the received AFM data. Microvilli are located on areas of cleavage furrows (Monroy et al., 1976). Microvilli are probably not presented on AFM images because they are situated particularly at the bottom of the cleavage furrows, so cantilever tip does not interact with them.

### 3.1.3. Gastrula (stage 10)

The ultrastructure of gastrula epithelium was visualized by AFM (Fig. 6A, B and E). Cells of the gastrula are smaller than the blastula cells. Cell boundaries on the animal pole appear as narrow eminences ( $120 \pm 60$  nm height,  $580 \pm 170$  width) at the bottom

of furrows (Fig. 6C). These eminences correspond to the places of tight cell junctions.

On the animal pole the visible yolk granules are almost lacking (Fig. 6A and B), on the vegetal pole their quantity does not change ( $13 \pm 5$  per  $100 \mu\text{m}^2$ ) (Fig. 7A and B). There are two types of superficial cells on the animal pole: covered by small blebs (less than  $1 \mu\text{m}$  size) and without them. So we interpret these blebs as microvilli (Fig. 6E), their density can be numerically estimated. The values, obtained from AFM and SEM images coincide quite closely ( $1.1 \pm 0.1 \mu\text{m}^{-2}$  and  $1.0 \pm 0.1 \mu\text{m}^{-2}$  respectively). As well as at blastula stage, artifacts of fixation (funnel-like deepenings with  $0.5\text{--}4 \mu\text{m}$  diameter) in the area of cell boundaries are visible

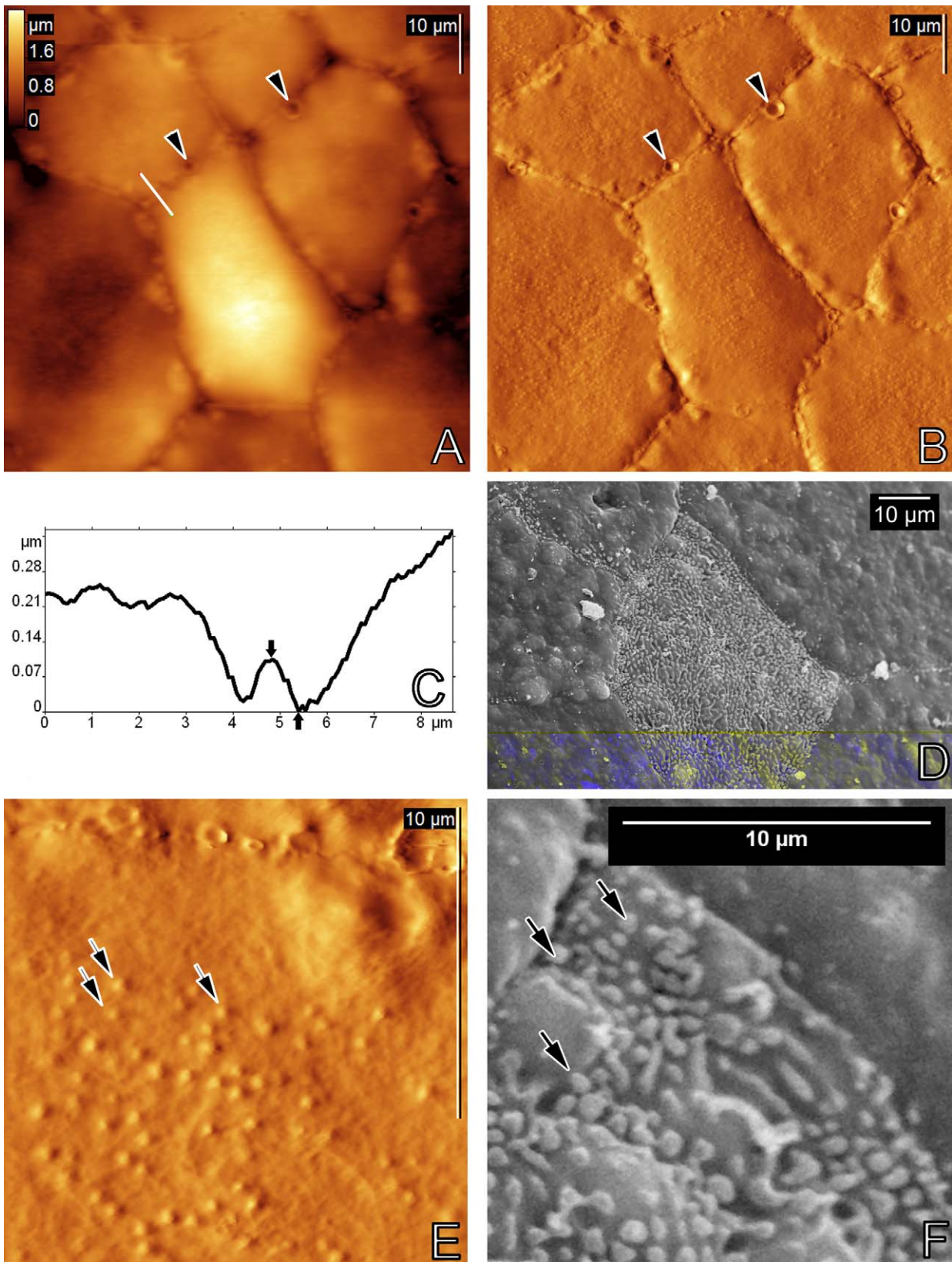


**Fig. 6.** Fixed gastrula (st. 10), animal pole, contact mode AFM in liquid. Microvilli are better visible in contact error images (B) and (E), than in topography (A). (C) Height profile of the white line in (A). The eminence indicated with arrows in (C) is 98 nm height. (D) and (F) Scanning electron micrograph. Arrows indicate the microvilli, triangular pointers show poles in the area of the cell boundaries.

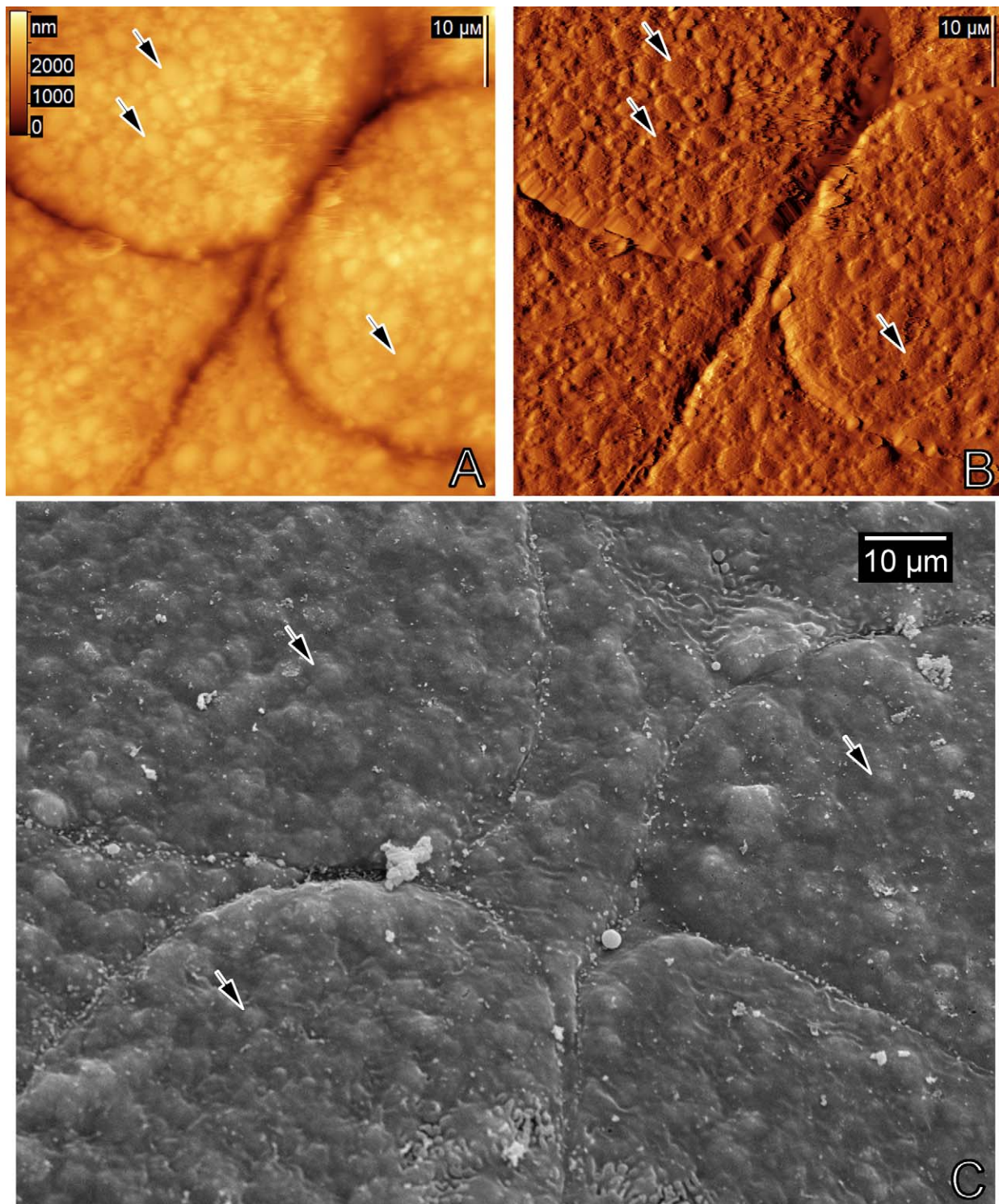


**Fig. 7.** Fixed gastrula (st. 10), vegetal pole, contact mode AFM in liquid: (A) topography and (B) error signal images. (C) Scanning electron micrograph. Arrows indicate some of the yolk granules.

(Monroy et al., 1976). The images of the vegetal pole of blastula and gastrula stages are similar, so only the gastrula images are shown.

#### 3.1.4. Neurula (stage 14)

At the neurula stage the neural tube forms, so the surface curvature increases. Large variations of height make it difficult to investigate the neurula surface with AFM. Therefore images were obtained only from the flattest regions of the embryo, which are the lateral surface and the anterior part of it (Fig. 2E).

The hemispherical bodies ( $\sim 700$  nm height,  $\sim 2$   $\mu$ m diameter) on the cell surface are visible (up to 3 per cell), we interpreted them as yolk granules (Fig. 8A and B). The number of the yolk granules decreases, so they are expanded during embryo development. Eminences at cell boundaries ( $620 \pm 170$  nm width and  $180 \pm 60$  nm height) are still visible at the neurula stage. The data is in agreement with SEM images (Fig. 8C) (Monroy et al., 1976; Tarin, 1971). Later stages were not investigated.

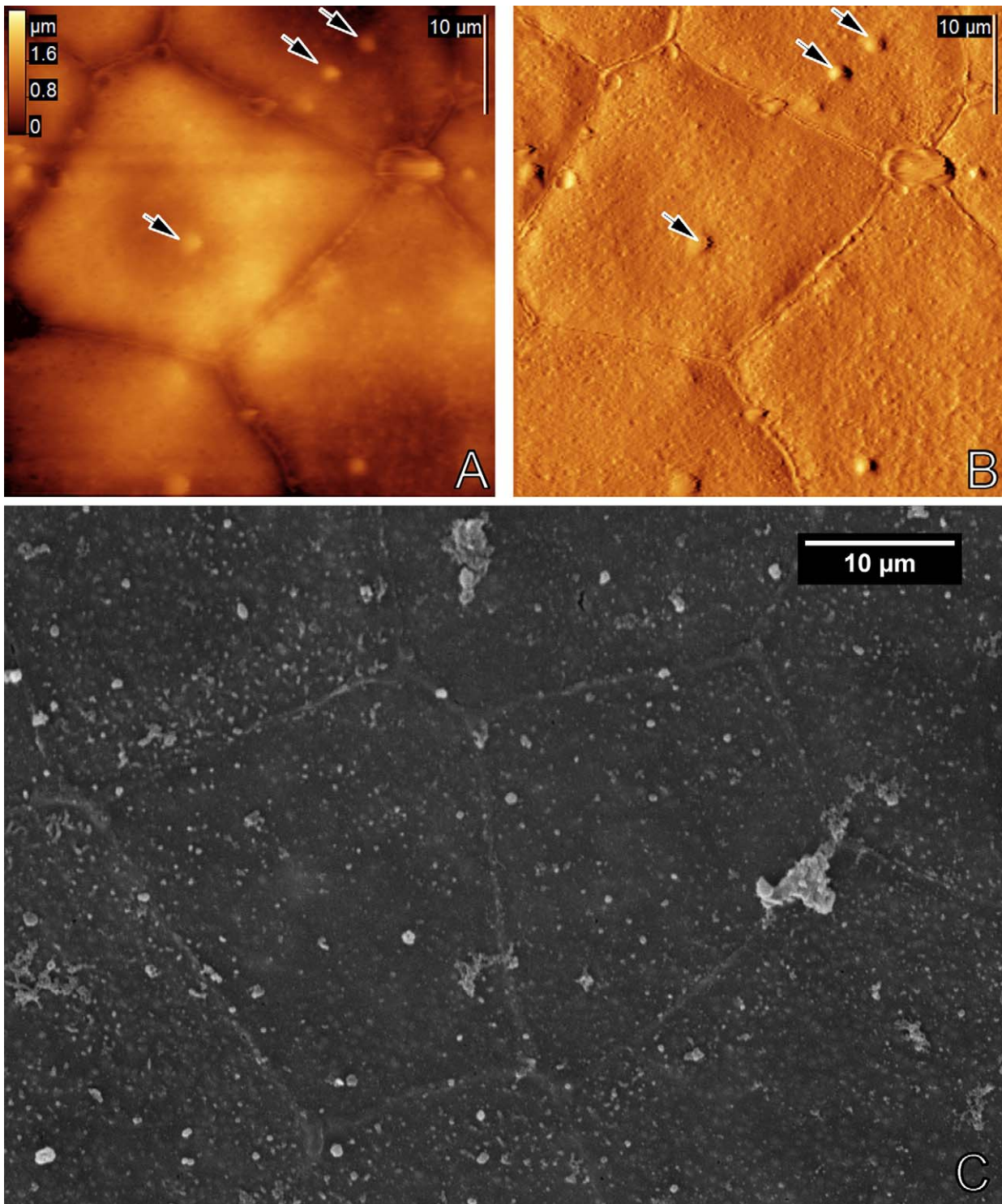


**Fig. 8.** Fixed neurula (st. 14), the lateral surface of an embryo, contact mode AFM in liquid: (A) topography and (B) error signal images. (C) Scanning electron micrograph. Arrows indicate some of the yolk granules.

The AFM images of fixed embryos' morphology confirm the SEM data in general. At gastrula and neurula stages AFM and SEM data are in good agreement, at blastula stage the cell borders and the yolk granules are visible on both AFM and SEM images, however we did not manage to observe the microvilli when the embryos were imaged in liquid by AFM. At the primary stages two distinct features can be observed by AFM: the yolk granules and the microvilli. The latter are not observed when the samples are imaged in liquid

but are clearly visible by AFM in air and SEM. Artifacts, which are presented on SEM images, are also visible on AFM images.

The procedure of sample preparation for AFM is faster and does not require complex and invasive sample treatments, such as additional fixation, dehydration, drying and metal coating that can significantly modify the native structure and cause artifacts. Furthermore, AFM allows one to perform more precise measurements on the z axis of the sample. On the other hand, AFM imaging is typi-

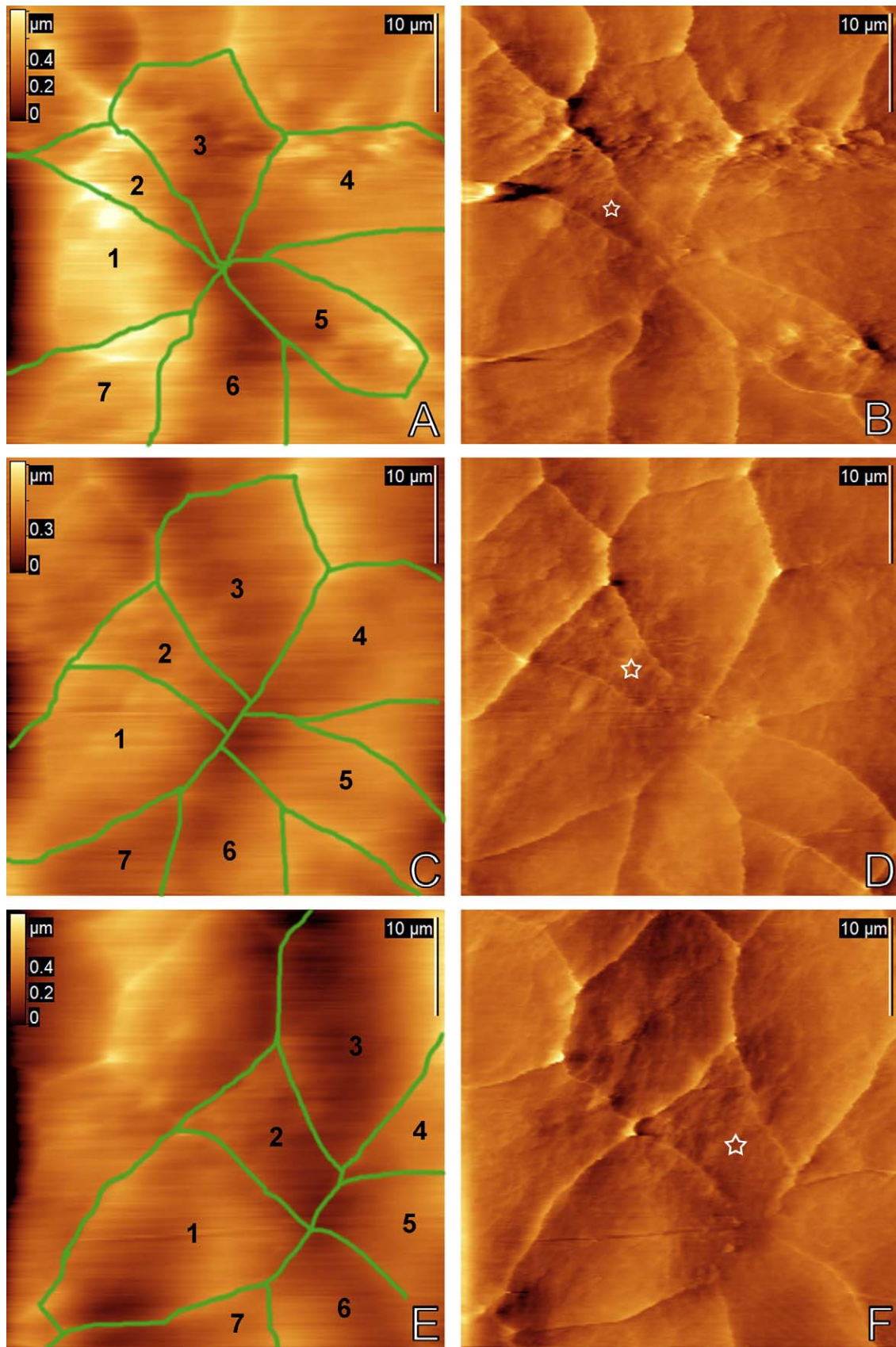


**Fig. 9.** A series of images shows the resolving of the rosette-like structure on the surface of living embryo (st. 11, animal pole), contact mode AFM in liquid. Topography (A, C, E) and corresponding error signal images (B, D, F). It takes ~5 min to obtain one image, images (A) and (C) obtained in succession, (C) and (E) are the next nearest. The cell marked by an asterisk gradually changes its shape. On the topographical images rosette boundaries are marked by green lines, and cells are numbered. (For interpretation of the references to color in this figure legend, the reader is referred to the web version of the article.)

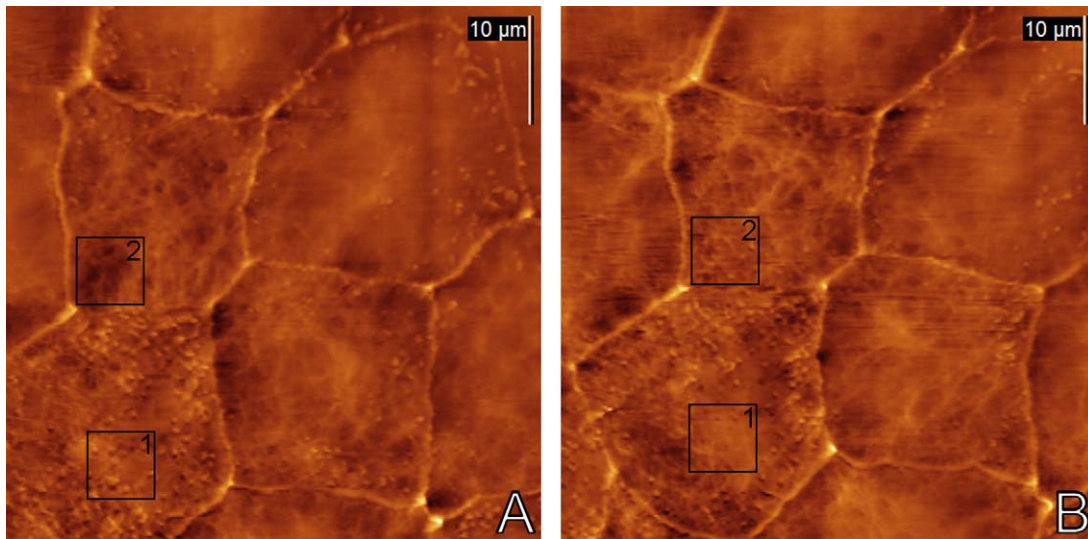


**Fig. 10.** Two consecutive contact error images (~5 min on each scan) of living embryo surface (st. 10, animal pole). The microvilli and cytoskeleton rearrangements are visible. In the area, indicated by box 1, microvilli disappeared. In the area, indicated by box 2, cytoskeleton rearranged and some microvilli-like protrusions appeared.

cally slower than SEM. On the whole, AFM and SEM can be regarded as substitutable techniques to study fixed embryos.

### 3.2. Research of living *X. laevis* embryos

The possibility of investigation of living objects in their physiological environment is the major advantage of AFM over many other methods of microscopy, in particular electron microscopy. However, imaging living objects by AFM has some difficulties. First, the sample has to be tightly adsorbed/held on a substrate and must not shift under the influence of forces from the cantilever. Second, if the sample is too soft, as the majority of biological objects, it will be difficult to achieve high resolution; also the sample can be damaged by the cantilever. Third, when studying the dynamic process, the rate of changes in the sample should be slower than the rate of image acquisition to observe them. These problems are usually hard to solve; therefore many living biological objects still have not been investigated by the AFM.

Despite such problems in this work the surface of a living embryo has been investigated by AFM. It is possible to receive a series of images of the same area of a sample surface and to visualize cellular rearrangements *in vivo* in real time. We have focused our investigation on the blastula and gastrula stages of development when intensive morphogenetic cell movements take place.

Cell rearrangements that occur during *X. laevis* gastrulation are a common mechanism of morphogenetic changes in embryonic tissues (Gerhart and Keller, 1986). One of the morphogenetic processes during the gastrulation is mesoderm cell involution in the area called blastopore (Fig. 2D). A radial intercalation of deeper cells into a more superficial cell layer is responsible for the epiboly, a morphogenetic process in which the ectodermal epithelium expands to cover a large surface of the embryo. Another morphogenetic process is convergent extension, which results from an oriented intercalation of cells toward the midline of the tissue axis and causes the tissue to narrow and elongate in the anterior–posterior direction. Convergent extension occurs in both epithelial and mesenchymal tissues. Several experiments argue that the forces driving convergent extension are generated by the deep, non-epithelial, mesenchymal cells and suggest that the epithelial sheets of both mesodermal and neural regions are passively stretched by the underlying, actively extending deep tissue. However, this area of the embryonic epithelium may be specialized in such a way, that passive cell rearrangement occurs more

easily than in other regions that normally do not converge and extend (Keller et al., 2008). Moreover, in order to rearrange within an epithelium, cells need to be able to rapidly break and, probably simultaneously, remake contacts with their neighbors without even creating disruptions in the permeability barrier provided by tight junctions (Gumbiner, 1992). Investigation of cell movements during morphogenesis is a complicated and challenging task.

A series of images showing cell rearrangements of a living gastrula-stage embryo is shown in Fig. 9. On topography images the cell boundaries look like eminences with a 1–2  $\mu\text{m}$  width and 50–100 nm height, in places of joints the height is up to 300 nm. Rosette-like structures are found in the epithelium at the animal pole of the gastrula (Fig. 9). Their role in the *X. laevis* development is poorly understood. Multi-cellular rosettes seem to be important during the ingression of cells following an epithelial to mesenchymal transition at the avian primitive streak, and during the germ band extension in *Drosophila* (Blankenship et al., 2006; Wagstaff et al., 2008).

In Fig. 9 we observe the continuous resolving of the rosette-like structure, visualized by AFM. The marked cell gradually changes its shape from a triangular to a square one. A similar process was observed by GFP-labeling of membrane proteins in *Drosophila* (Blankenship et al., 2006). The average speed of relative boundary movements measured by AFM (the rate of elongation (or shortening) of the cell boundary fragments) is  $\sim 0.5\text{--}1.5 \mu\text{m}/\text{min}$ . This estimate is in agreement with data from time-lapse cinemicrography: the rate of the cells translocation near the blastopore is about 1.8–4  $\mu\text{m}/\text{min}$  (Keller, 1978). Hence, AFM is a good method for the investigation of cell movements within the embryo without any additional preparation.

When soft matter is studied by AFM the lateral resolution is determined by the elasticity of the samples, and for living cells (typical elasticity is 1–10 kPa) it is on the order of hundreds nm (Braet et al., 1998). The vertical resolution is typically better and constitutes tens nm or less. So, small surface elements, like microvilli, can be visualized on living embryos.

Besides cell rearrangement it is possible to see other changes of surface structure. On the deflection images (contact error signal), microvilli and submembrane cytoskeleton are visible (Fig. 10). Microvilli look like small knobs (approximately 50 nm height on topography images) less than 1  $\mu\text{m}$  in diameter, and have density  $0.8 \pm 0.1 \mu\text{m}^{-2}$ , which is close to the value measured on the fixed samples (see above). Microvilli are mostly located close to the cell

boundaries, but some cells are entirely covered by them. During continuous imaging it is possible to observe changes of quantity of microvilli and their displacement on the cell surface. The network which is visible on the surface can be interpreted as the cytoskeleton (Santacroce et al., 2006). It is frequently observed with AFM in contact error mode (Braet and Wisse, 2004). The cytoskeleton of an embryo is a very dynamic structure, so we can visualize its changes *in vivo*, as it is shown on Fig. 10. These changes appear as alteration in location of holes, risings, fibers on the surface. Similar morphological structure of cortical actin network was visualized with confocal laser scanning microscopy (Skoglund et al., 2008).

In this work AFM-images of cell rearrangement in living embryos have been received for the first time. Similar time-lapse images were obtained earlier by time-lapse cinemicrography (Keller, 1978; Wallingford, 2010) and confocal laser scanning microscopy (Kieserman et al., 2010). Both methods provide fast image acquisition of the living embryo surface. However, time-lapse microscopy typically has a low resolution and confocal laser scanning microscopy requires fluorescent labeling of specific proteins through gene transformation (Blankenship et al., 2006; Davidson et al., 2008). So AFM has certain advantages: easy sample preparation, ability to obtain 3D images, good resolution (it was possible to observe 50 nm height microvilli on the living embryo surface). It should be pointed out that the embryo develops normally after AFM analysis – this confirms that AFM is a low invasive method.

#### 4. Conclusions

In our work it is shown that AFM can be used as an instrument to study amphibian embryo surface at different stages of its development. New sample preparation protocol was used for these observations.

Investigation of fixed embryos by AFM allows us to obtain data analogous to SEM, but does not require complex sample preparation and treatment. AFM images obtained in liquid and SEM images are similar when the studied embryo is at gastrula and neurula stages, but slightly different at primary stages and blastula.

We have shown that AFM can be applied to study cell movements on the embryo surface *in vivo* as well as to visualize changes of quantity and distribution of microvilli on cell surface and cytoskeleton remodeling. Our findings allow us to recommend AFM as a tool to study the influence of various drugs/bioactive compounds on these processes (after addition of the studied substances to the cultivation medium). In the future we plan to use AFM to measure local module of elasticity of embryos.

#### Acknowledgments

This work was supported by the federal target program “Scientific and educational research personnel to innovative Russia” and Russian Fond for Fundamental Investigations (RFFI); Grant number: 05-04-48681. The authors thank Professor L.V. Belousov and N.N. Luchinskaya for their skilled consultations, Ms. Lisa Trifonova and K.A. Michurina for proofreading the manuscript.

#### Appendix A. Supplementary data

Supplementary data associated with this article can be found, in the online version, at doi:10.1016/j.micron.2011.05.010.

#### References

Ando, T., Koderu, N., Naito, Y., Kinoshita, T., Furuta, K., Toyoshima, Y.Y., 2003. A high speed atomic force microscope for studying biological macromolecules in action. *ChemPhysChem* 4, 1196–1202.

- Blankenship, J.T., Backovic, S.T., Sanny, J.S.P., Weitz, O., Zallen, J.A., 2006. Multicellular rosette formation links planar cell polarity to tissue morphogenesis. *Dev. Cell* 11, 459–470.
- Braet, F., Rotsch, C., Wisse, E., Radmacher, M., 1998. Comparison of fixed and living liver endothelial cells by atomic force microscopy. *Appl. Phys. A: Mater. Sci. Process.* 66, 575–578.
- Braet, F., Wisse, E., 2004. Imaging surface and submembranous structures in living cells with the atomic force microscope: notes and tricks. *Methods Mol. Biol.* (Clifton, NJ) 242, 201–217.
- Butt, H.J., Cappella, B., Kappl, M., 2005. Force measurements with the atomic force microscope: technique, interpretation and applications. *Surf. Sci. Rep.* 59, 1–152.
- Cai, X., Gao, S., Cai, J., Wu, Y., Deng, H., 2009. Artesunate induced morphological and mechanical changes of Jurkat cell studied by AFM. *Scanning* 31, 83–89.
- Davidson, L.A., Dzamba, B.D., Keller, R., Desimone, D.W., 2008. Live imaging of cell protrusive activity, and extracellular matrix assembly and remodeling during morphogenesis in the frog, *Xenopus laevis*. *Dev. Dyn.* 237, 2684–2692.
- Denis-Donini, S., Baccetti, B., Monroy, A., 1976. Morphological changes of the surface of the eggs of *Xenopus laevis* in the course of development. 2. Cytokinesis and early cleavage. *J. Ultrastruct. Res.* 57, 104–112.
- Engel, A., Muller, D.J., 2000. Observing single biomolecules at work with the atomic force microscope. *Nat. Struct. Mol. Biol.* 7, 715–718.
- Gerhart, J., Keller, R., 1986. Region-specific cell activities in amphibian gastrulation. *Annu. Rev. Cell Biol.* 2, 201–229.
- Graham, H.K., Hodson, N.W., Hoyland, J.A., Millward-Sadler, S.J., Garrod, D., Scothern, A., Griffiths, C.E.M., Watson, R.E.B., Cox, T.R., Erler, J.T., 2010. Tissue section AFM: in situ ultrastructural imaging of native biomolecules. *Matrix Biol.* 29, 254–260.
- Gumbiner, B.M., 1992. Epithelial morphogenesis. *Cell* 69, 385.
- Gurdon, J.B., Hopwood, N., 2000. The introduction of *Xenopus laevis* into developmental biology: of empire, pregnancy testing and ribosomal genes. *Int. J. Dev. Biol.* 44, 43–50.
- Jurvelin, J., Mjler, D., Wong, M., Studer, D., Engel, A., Hunziker, E., 1996. Surface and subsurface morphology of bovine humeral articular cartilage as assessed by atomic force and transmission electron microscopy. *J. Struct. Biol.* 117, 45–54.
- Kay, B., 1991. *Xenopus laevis*: practical uses in cell and molecular biology. Injections of oocytes and embryos. *Methods Cell Biol.* 36, 663–672.
- Keller, R., 1975. Vital dye mapping of the gastrula and neurula of *Xenopus laevis*. I. Prospective areas and morphogenetic movements of the superficial layer. *Dev. Biol.* 42, 222–263.
- Keller, R., 1978. Time-lapse cinemicrographic analysis of superficial cell behavior during and prior to gastrulation in *Xenopus laevis*. *J. Morphol.* 157, 223–247.
- Keller, R., 1980. The cellular basis of epiboly: an SEM study of deep-cell rearrangement during gastrulation in *Xenopus laevis*. *J. Embryol. Exp. Morphol.* 60, 201–234.
- Keller, R., 1981. An experimental analysis of the role of bottle cells and the deep marginal zone in gastrulation of *Xenopus laevis*. *J. Exp. Zool.* 216, 81–101.
- Keller, R., Davidson, L., Edlund, A., Elul, T., Ezin, M., Shook, D., Skoglund, P., 2000. Mechanisms of convergence and extension by cell intercalation. *Philos. Trans. Royal Soc. Lond. B: Biol. Sci.* 355, 897–922.
- Keller, R., Shook, D., Skoglund, P., 2008. The forces that shape embryos: physical aspects of convergent extension by cell intercalation. *Phys. Biol.* 5, 015007.
- Kieserman, E., Lee, C., Gray, R., Park, T., Wallingford, J., 2010. High-magnification *in vivo* imaging of *Xenopus* embryos for cell and developmental biology. In: *Cold Spring Harb. Protoc.* 2010, pdb. prot5427.
- Kreplak, L., Wang, H., Aebi, U., Kong, X.P., 2007. Atomic force microscopy of mammalian urothelial surface. *J. Mol. Biol.* 374, 365–373.
- Kuznetsova, T.G., Starodubtseva, M.N., Yegorenkov, N.I., Chizhik, S.A., Zhdanov, R.I., 2007. Atomic force microscopy probing of cell elasticity. *Micron* 38, 824–833.
- Lal, R., Yu, L., 1993. Atomic force microscopy of cloned nicotinic acetylcholine receptor expressed in *Xenopus* oocytes. *Proc. Natl. Acad. Sci. USA* 90, 7280–7284.
- Lau, J.M., You, H.X., Yu, L., 2002. Lattice-like array particles on *Xenopus* oocyte plasma membrane. *Scanning* 24, 224–231.
- Miyazaki, H., Hayashi, K., 1999. Atomic force microscopic measurement of the mechanical properties of intact endothelial cells in fresh arteries. *Med. Biol. Eng. Comput.* 37, 530–536.
- Monroy, A., Baccetti, B., 1975. Morphological changes of the surface of the egg of *Xenopus laevis* in the course of development: I. Fertilization and early cleavage. *J. Ultrastruct. Res.* 50, 131–142.
- Monroy, A., Baccetti, B., Denis-Donini, S., 1976. Morphological changes of the surface of the egg of *Xenopus laevis* in the course of development: III. Scanning electron microscopy of gastrulation. *Dev. Biol.* 49, 250–259.
- Nieuwkoop, P.D., Faber, J., Gurdon, J.B., 1967. Normal Table of *Xenopus laevis* (Daudin). North-Holland Publ. Co, Amsterdam.
- Oberleithner, H., Schillers, H., Wilhelmi, M., Butzke, D., Danker, T., 2000. Nuclear pores collapse in response to CO<sub>2</sub> imaged with atomic force microscopy. *Pflug. Arch. Eur. J. Physiol.* 439, 251–255.
- Orsini, F., Santacroce, M., Arosio, P., Castagna, M., Lenardi, C., Poletti, G., Sacchi, F., 2009. Intermittent contact mode AFM investigation of native plasma membrane of *Xenopus laevis* oocyte. *Eur. Biophys. J.* 38, 903–910.
- Orsini, F., Santacroce, M., Arosio, P., Sacchi, V.F., 2010. Observing *Xenopus laevis* oocyte plasma membrane by atomic force microscopy. *Methods* 51, 106–113.
- Orsini, F., Santacroce, M., Perego, C., Lenardi, C., Castagna, M., Mari, S., Sacchi, V., Poletti, G., 2006. Atomic force microscopy characterization of *Xenopus laevis* oocyte plasma membrane. *Microsc. Res. Tech.* 69, 826–834.
- Reichlin, T., Wild, A., Durrenberger, M., Daniels, A., Aebi, U., Hunziker, P.R., Stolz, M., 2005. Investigating native coronary artery endothelium *in situ* and in cell culture by scanning force microscopy. *J. Struct. Biol.* 152, 52–63.

- Ricci, D., Braga, P.C., 2004. Recognizing and avoiding artifacts in AFM imaging. *Methods Mol. Biol.* 242, 25–38.
- Rotsch, C., Jacobson, K., Radmacher, M., 1999. Dimensional and mechanical dynamics of active and stable edges in motile fibroblasts investigated by using atomic force microscopy. *Proc. Natl. Acad. Sci. USA* 96, 921–927.
- Rotsch, C., Radmacher, M., 2000. Drug-induced changes of cytoskeletal structure and mechanics in fibroblasts: an atomic force microscopy study. *Biophys. J.* 78, 520–535.
- Santacroce, M., Orsini, F., Mari, S.A., Marinone, M., Lenardi, C., Bett, S., Sacchi, V.F., Poletti, G., 2008. Atomic force microscopy imaging of *Xenopus laevis* oocyte plasma membrane purified by ultracentrifugation. *Microsc. Res. Tech.* 71, 397–402.
- Santacroce, M., Orsini, F., Perego, C., Lenardi, C., Castagna, M., Mari, S., Sacchi, V., Poletti, G., 2006. Atomic force microscopy imaging of actin cortical cytoskeleton of *Xenopus laevis* oocyte. *J. Microsc.* 223, 57–65.
- Schillers, H., Danker, T., Schnittler, H.J., Lang, F., Oberleithner, H., 2000. Plasma membrane plasticity of *Xenopus laevis* oocyte imaged with atomic force microscopy. *Cell. Physiol. Biochem.* 10, 99–107.
- Shahin, V., Albermann, L., Schillers, H., Kastrup, L., Sch fer, C., Ludwig, Y., Stock, C., Oberleithner, H., 2005. Steroids dilate nuclear pores imaged with atomic force microscopy. *J. Cell. Physiol.* 202, 591–601.
- Skoglund, P., Rolo, A., Chen, X., Gumbiner, B.M., Keller, R., 2008. Convergence and extension at gastrulation require a myosin IIB dependent cortical actin network. *Development* 135, 2435–2444.
- Solletti, J.M., Kasas, S., Bertrand, D., Weisenhorn, A., 1994. Atomic force and scanning electron microscopy of *Xenopus laevis* oocytes. *J. Vac. Sci. Technol. B: Microelectron. Nanometer Struct.* 12, 1535–1538.
- Suzuki, Y., Yokokawa, M., Yoshimura, S.H., Takeyasu, K., 2011. Biological application of fast-scanning atomic force microscopy. *Scanning Probe Microsc. Nanosci. Nanotechnol.* 2, 217–246.
- Tarin, D., 1971. Scanning electron microscopical studies of the embryonic surface during gastrulation and neurulation in *Xenopus laevis*. *J. Anat.* 109, 535–582.
- Tsilimbaris, M.K., Lesniewska, E., Lydataki, S., Le Grimellec, C., Goudonnet, J.P., Pallikaris, I.G., 2000. The use of atomic force microscopy for the observation of corneal epithelium surface. *Invest. Ophthalmol. Vis. Sci.* 41, 680–686.
- Vinckier, A., Semenza, G., 1998. Measuring elasticity of biological materials by atomic force microscopy. *FEBS Lett.* 430, 12–16.
- Wagstaff, L.J., Bellett, G., Mogensen, M.M., Munsterberg, A., 2008. Multicellular rosette formation during cell ingression in the avian primitive streak. *Dev. Dyn.* 237, 91–96.
- Wallingford, J., 2010. Low-magnification live imaging of *Xenopus* embryos for cell and developmental biology. In: Cold Spring Harb. Protoc. 2010, pdb. prot5425.